Low-Order Modeling of Resonance for Fixed-Valve Micropumps Based on First Principles

Christopher J. Morris, *Member, ASME,* and Fred K. Forster, *Member, ASME*

***Abstract*—Micropumps that utilize fixed-valves, i.e., valves having no moving parts, are relatively easy to fabricate and inherently reliable due to their simplicity. Since fixed-valves do not close, pumps based on them need to operate in a well-designed resonant mode in order to attain flow rates and pressures comparable with other designs. However, no methodology currently exists to efficiently investigate all the design parameters including valve *size* to achieve optimal resonant response. A methodology that addresses this problem is 1) the determination of optimal parameters including valve *size* with a low-order linear model capable of nonempirical prediction of resonant behavior, and 2) the independent determination of the best valve *shape* for maximal valve action over a target Reynolds number range. This study addresses the first of these two steps. The hypothesis of this study is that the resonant behavior of a fixed-valve micropump can be accurately predicted from first principles, i.e., with knowledge only of geometric parameters and physical constants. We utilized a new low-order model that treats the valves as straight rectangular channels, for which the unsteady solution to the Navier-Stokes equations is exact and with which the problem was linearized. Agreement with experiment using pump-like devices with valves replaced by straight channels was found to be excellent, thereby demonstrating the efficacy of the model for describing all aspects of the pump except actual valves. Agreement with experiment using pumps with Tesla-type valves was within 20 percent. With such accuracy and without the need for empirical data, the model makes possible reliable, efficient investigation and optimization of over 30 geometric and material parameters. [762]**

***Index Terms*—Diffuser, electrical-equivalent model, fixed-valve, low-order model, lumped parameters, macromodel, micropump, nozzle-diffuser, Tesla.**

I. Introduction

MICROFLUIDICS is an increasingly important area of MEMS, with applications in chemical synthesis, chemical detection, microbiology, biological detection, clinical analysis in medicine, and heat transfer in microelectrical devices. A fundamental component of a self-contained microfluidic system is a pump.

Numerous research groups have been active in developing micropumps. Typical designs are positive displacement pumps that rely on valves. Valves are often passive such as floating-ball check valves [1], or cantilever-beam "flapper-valves" [2], [3].

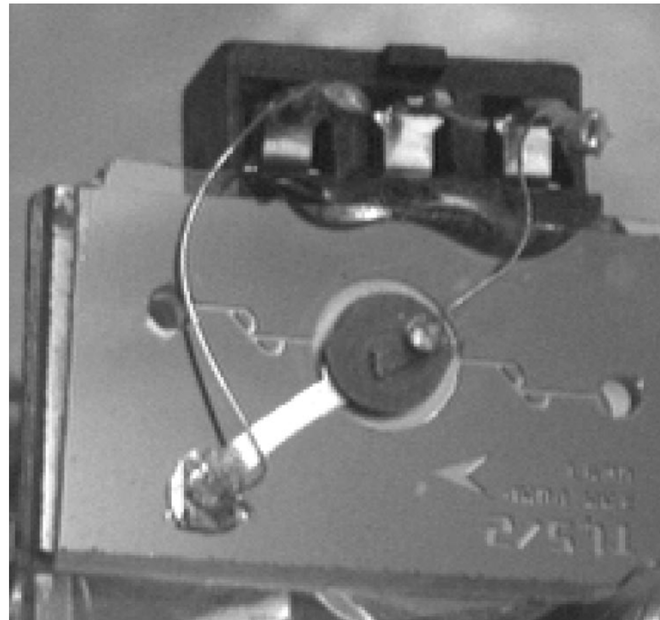

Fig. 1. Fixed-valve micropump with a 3 mm diameter chamber and 114 μm wide channels. The channels operate as valves, providing a higher pressure drop in the reverse (left-to-right) than in the forward direction.

Some designs have flapper valves directly under the pump actuator to take advantage of the same actuation, creating partly-active, partly-passive valves [4], [5].

A particular class of micropumps employs fixed-valves. Such valves do not open and close, but due to their shape alone provide less flow resistance in one direction compared to that in the opposite direction. For example, a converging-diverging axisymmetric nozzle-diffuser valve was demonstrated by Stemme and Stemme in a mesoscale pump [6]. A simple diffuser valve etched in silicon and oriented out-of-plane was studied by Gerlach and Wurmus [7]. A silicon-etched nozzle-diffuser valve oriented in-plane was reported by Forster *et al.* [8], [9] along with a micropump based on Tesla-type valves [10], as shown in Fig. 1. The fixed-valve micropump is relatively simple to fabricate. Also, since fixed-valves typically have clearances significantly greater than corresponding mechanical valves, they allow the transport of relatively large particles [11], [12]. Another advantage of fixed-valves is more freedom for design of pump resonance, because the operating frequency is not limited by the time needed for mechanical valves to open and close.

The efficient design of micropumps requires some form of modeling. Large degree-of-freedom modeling, such as finite element structural analysis or computational fluid dynamics,

Manuscript received September 25,2001; revised November 12,2002. This work was supported in part by DARPA Microflumes Program contract N66001-97-C-8632, DARPA Composite CAD Program contract F30602-98-2-0151 and graduate fellowships from the NASA Space Grant and the Boeing Company. Subject Editor D. Cho.

The authors are with the Mechanical Engineering Department, University of Washington, Seattle, WA 98195-2600 USA (e-mail: cjmorris@u.washington.edu; forster@u.washington.edu).

Digital Object Identifier 10.1109/JMEMS.2003.809965

1057-7157/03$17.00 © 2003 IEEE

has merit for understanding details about certain components. But low-order modeling, where a system is represented by a small number of discrete elements such as masses and resistors, can be advantageous for understanding the behavior and design of entire pump systems. Due to electromechanical and mechanical-fluid coupling, large degree of freedom modeling is impractical for design and optimization of time-dependent systems—especially fixed-valve pumps, which typically operate in the kilohertz frequency range.

Several authors have considered low-order nonlinear models for micropumps with mechanical valves [13]–[15]. For fixed-valve micropumps, Olsson *et al.* [16], Ullman *et al.* [17] and Olsson *et al.* [18] present nonlinear models of diffuser pumps, which show a progression of complexity, and all of which require numerous assumptions and empirical coefficients. In [18] very good agreement is shown between experiment and simulation. However, for each prototype pump simulated, valve characteristics specific to each pump are described with relations that include seven coefficients, five of which are derived from steady flow experiments, and two of which are adjusted for the best fit to the data for the unsteady case. In addition, ad hoc expressions for velocity profiles for both laminar and turbulent flow are included. While such exercises demonstrate the power of simulation tools, the ability to predict performance useful for design has not been demonstrated. More importantly, parameter adjustments in one area of a model may simply mask errors in another.

An alternative approach to designing fixed-valve micropumps is to divide the overall design methodology into two parts. The first part consists of a low-order, linearized model for use in maximizing resonant behavior through optimization of all pertinent parameters including valve *size*. Such a model is not able to predict net pressure and flow characteristics, but rather relate the geometric and material properties of pump components to the resonant frequency and amplitude of oscillation. The second part determines optimum valve *shape* to maximize pump performance in terms of net pressure and flow, i.e., the nonlinear pump characteristics. Following this methodology, a linear electrical-equivalent network for fixed-valve pumps is discussed by Bardell *et al.* [19] and Forster *et al.* [20]. The authors use linear modeling to optimize pump membrane thickness for a given valve and demonstrate that "stiffening" an existing design can improve resonance and therefore pump performance in terms of net pressure and flow rate. The predictive value of the particular model reported and thus the usefulness for design optimization was, however, limited due to the experimental determination of several model parameters.

The hypothesis of this study is that the resonant behavior of fixed-valve micropumps can be predicted from first principles alone. This means the only inputs necessary are geometric and material properties. This study extends our previous work reported in [19], [20] by utilizing finite element analysis to determine low-order element values that represent the mechanical and electrical portions of the pump. One entirely new aspect of this study is that it utilizes the exact solution for oscillatory flow in straight rectangular channels to obtain values for the fluidic elements. Although straight-channel fluid flow behavior is only an approximation of the more complex flow in actual valves, the differential behavior of fixed-valves at the relatively low Reynolds number associated with micropumps is small compared to mechanical valves [8]. One purpose of this study is to investigate whether the nonlinear valve behavior can be neglected for predictions of resonant pump behavior. In addition, the important role of both viscous and inertial effects throughout the frequency range are properly taken into account with the exact solution to the Navier-Stokes equations, a factor that has not been considered in other modeling efforts. This is critically important when the combination of pump parameters is such that the pump operating frequency is in the vicinity of the valve cutoff frequency.

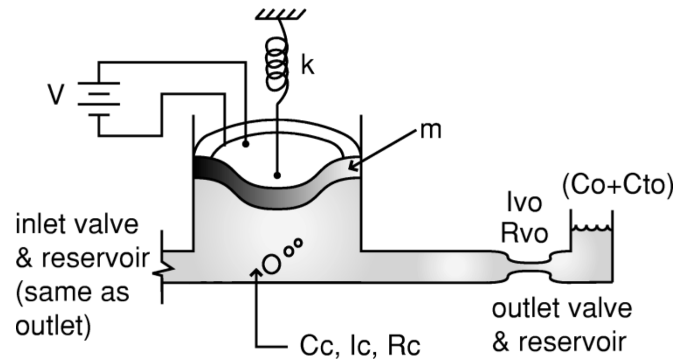

Fig. 2. Schematic diagram showing the discrete elements associated with the fixed-valve micropump in Fig. 1, or the straight-channel device shown in Fig. 6.

II. Methods

In this study a linear, low-order, state-space model was developed, for which all the discrete model parameters were determined from first principles. To investigate the accuracy of the approach, "micropump-like" devices with valves replaced by straight channels were utilized. Fully operational micropumps with fixed-valves of the Tesla-type were also used. The model, physical devices, and experimental procedures are described below.

A. Low-Order Model

The low-order model used to describe the dynamic behavior of micropumps such as that shown in Fig. 1 was based on the schematic diagram shown in Fig. 2. The linear graph [21] shown in Fig. 3 is defined by 15 discrete elements including those associated with the coupling elements between the electrical, mechanical and fluid domains [9], [19]. These parameters were derived from at least 36 different geometric and physical properties. The methods by which each element was determined are described below. A state-space model corresponding to the linear graph in Fig. 3 was implemented in Matlab (v5.3, The Mathworks, Inc., Natick, MA) to solve for various output variables in the frequency domain. The primary output variable utilized in this study was the centerline velocity amplitude of the membrane. The dynamic response of the membrane was chosen over flow rate of pumped fluid for a number of reasons. First, important information was obtained about the mechanical parameters of the pumps from free-air resonance of the device, i.e., with the pump empty of liquid. Second,

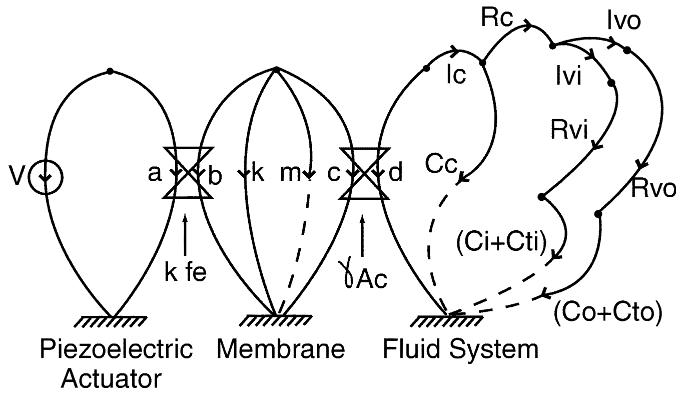

Fig. 3. Linear graph derived from the schematic diagram in Fig. 2, representing a fixed-valve micropump whose inlet and outlet are connected to open fluid reservoirs by tubing that is significantly larger than the valves.

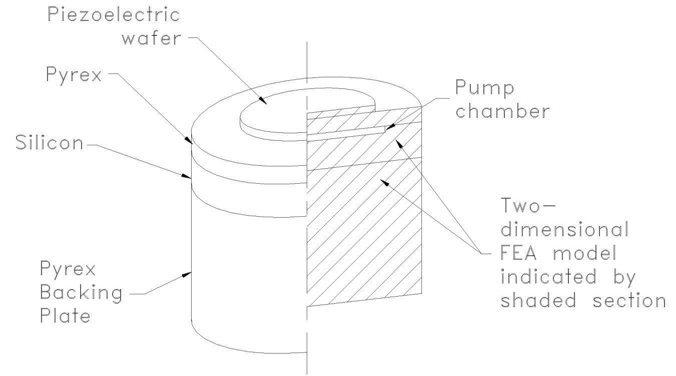

Fig. 4. Finite element model geometry for the axisymmetric plane of a circular, single-actuator layer bimorph.

accurate noninvasive measurement of instantaneous fluid flow rate at the pump outlet would be extremely difficult if not impossible. Finally, the accuracy of vibrometer measurements of membrane velocity even at displacements of a few micron is excellent.

1) Electromechanical Parameters: A review of the literature reveals that the deceptively simple case of a circular, single-layer piezoelectric bimorph is a difficult analytical problem [22], [23]. The presence of a bonding layer between the actuator and substrate and the ability to account for non-ideal edge conditions further complicate the problem [22]. Thus, the electrical and mechanical lumped parameters were determined from finite element analysis (FEA) using ANSYS 5.5 (Canonsburg, PA), which utilizes the same equations that would govern an analytical solution.

The pumps in this study had circular chambers, so a two-dimensional axisymmetric model of the piezoelectric bimorph was developed based on the geometry of the pump actuator shown in Fig. 4. The bimorph was modeled as PZT-5A bonded to Pyrex with conductive epoxy. The membrane support structure included the silicon pump housing. A Pyrex backing plate was also modeled. The material properties of the silicon, Pyrex and epoxy were characterized by Young's modulus E and Poisson's ratio ν. Silicon was modeled with $E = 1.3 \times 10^{11}$ Pa and $\nu = 0.22$ [24], Pyrex (Borofloat, US Precision Glass, Elgin, Illinois) with $E = 6.1 \times 10^{10}$ Pa and $\nu = 0.2$ and epoxy (EPO-TEK H31, Epoxy Technology, Billerica, Massachusetts) with $E = 5.17 \times 10^{9}$ Pa and Poisson's ratio $\nu = 0.3$. The material properties of PZT-5A (PSI-5A-S2, Piezo Systems, Cambridge, MA) and further details of the analysis are reported elsewhere [22].

The spring constant k was calculated based on chamber pressure P_c acting on the inside surface of the membrane of area A_c and given by

$$k = \frac{\gamma A_c P_c}{\delta_{\mathrm{mem}}} \qquad (1)$$

where δ_{mem} is the centerline displacement of the interior surface of the membrane. The shape factor γ is the ratio of the volume ΔV_{mem} displaced by the membrane to the volume that would be displaced by a piston having the same centerline displacement

$$\gamma = \frac{\Delta V_{\mathrm{mem}}}{A_c \delta_{\mathrm{mem}}}, \quad 0 < \gamma \le 1. \qquad (2)$$

It was calculated based on the volume swept by the inner surface of the elastic membrane due to voltage applied across the piezoelectric element as determined by the finite element analysis. The displacement-per-volt f_e was determined from the relation

$$f_e = \frac{\delta_{\mathrm{mem}}}{V} \qquad (3)$$

where here δ_{mem} was the calculated displacement for a given voltage V applied across the piezoelectric actuator. In the linear graph the product kf_e is the gyrator constant coupling the electrical and mechanical components. The product γA_c is the gyrator constant coupling the mechanical and fluid components. The equivalent mass m associated with the bimorph was calculated using a modal analysis feature of the finite element model. The resulting fundamental free-air resonant frequency ω_n of the membrane system was obtained, and m determined from the relation

$$m = \frac{k}{\omega_n^2}. \qquad (4)$$

2) Fluidic Chamber Parameters: The chamber dimensions for the pumps in this study were such that the resistance R_c and inductance I_c were negligible. These parameters could become significant for a deep chamber characterized by boundary layer flow along the vertical chamber walls, or for a very shallow chamber characterized by radial flow along the horizontal chamber surfaces.

The chamber capacitance was attributed to the compliance of the fluid in the chamber $(C_c)_f$ and from the flexibility of the chamber housing, $(C_c)_h$ such that

$$C_c = (C_c)_f + (C_c)_h. \qquad (5)$$

The pump housing capacitance was calculated using the finite element model outlined in Section II-A1). The total change in

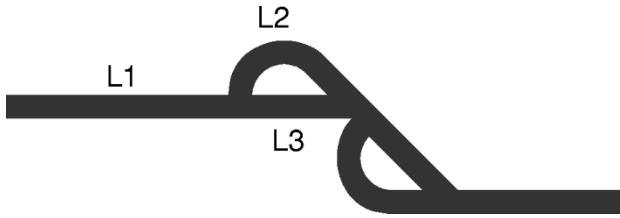

Fig. 5. Diagram showing a typical Tesla-type valve and two definitions of valve length. For $L \simeq L_{\rm eq}$ segments were combined as parallel and series impedances, i.e., $L_{\rm eq} = L1 + (1/L2 + 1/L3)^{-1} + \cdots$. For $L \simeq L_{\rm ave}$ the shortest and longest path through the valve were averaged, i.e., $L_{\rm ave} = (L_1 + L_3 + \cdots + L_1 + L_2 + \cdots)/2$.

chamber volume ΔV_c due to a chamber pressure P_c was calculated as

$$\Delta V_c = \Delta V_{\rm mem} + \Delta V_{\rm housing} \tag{6}$$

where $\Delta V_{\rm mem}$ is due to the displacement of the membrane. When ΔV_c is divided by P_c to form the expression of capacitance, $\Delta V_{\rm mem}/P_c$ can be expressed as $(\gamma A_c)^2/k$ by using (1), i.e., $\Delta V_{\rm mem}$ is already accounted for by the spring constant parameter, k. Thus, $(C_c)_h$ is the remaining term in (6), or

$$(C_c)_h = \frac{\Delta V_{\rm housing}}{P_c}. \tag{7}$$

Capacitance $(C_c)_f$ of the pumped fluid involved the compressibility effects of liquid and gas. The bulk modulus β of pumped liquid leads to the contribution V_c/β, where V_c is the chamber volume. The contribution due to gas based on adiabatic compression is given by $\phi V_c/\kappa P_c$, where ϕ is the effective volume of gas per unit volume of liquid and κ is the ratio of specific heats. The two effects are additive, and

$$(C_c)_f = \left(\frac{1}{\beta} + \frac{\phi}{\kappa P_c}\right) V_c. \tag{8}$$

If the pumped fluid were entirely gas, the first term in the above expression would not be included, and $\phi = 1$. For this study $\beta = 2.19 \times 10^9$ Pa for water and $\kappa = 1.4$ for air [25]. A consistent procedure was used to condition the working fluid such that ϕ was considered constant. The gas volume fraction ϕ is difficult to measure directly. In this study it was determined from experiments on "micropump-like" devices with straight channels replacing valves under conditions for which it was considered the only unknown parameter.

3) Fluidic Valve Parameters: The inlet and outlet valve resistance R_v and inductance I_v, were taken to be the same, i.e., $R_{vi} = R_{vo}$ and $I_{vi} = I_{vo}$ (see Fig. 3). The impedance of fluid channels

$$\widehat{Z}_v = \frac{\Delta \widehat{P}}{\widehat{Q}} = R_v + i\omega I_v \tag{9}$$

where $\Delta \widehat{P}$ and $\widehat{Q}$ are complex pressure drop and volume flow rate amplitudes and ω is radian frequency, is often described elsewhere by an approximation in which both R_v and I_v are independent of ω. For this ad hoc approximation, resistance corresponds to steady, viscous flow, and inertance corresponds to unsteady, inviscid flow. For a rectangular duct they are

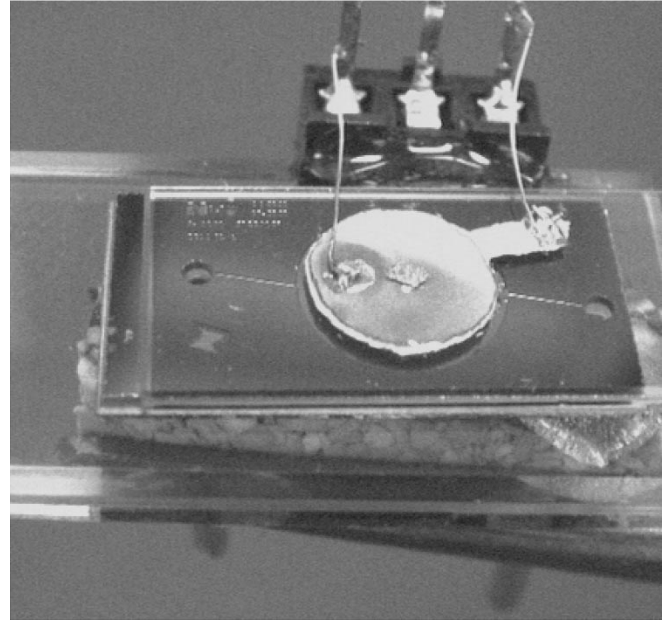

Fig. 6. A 6-mm-diameter chamber with 120 μm wide straight channels on each side. Etch depths for three different devices studied ranged from 115 μm to 152 μm. These devices were identical in fabrication to pumps such as shown in Fig. 1 except the valves were replaced with straight channels.

$$R_v = \frac{3\mu L}{4\alpha^3 b^4}\left[1 - 6\sum_{n=0}^{\infty}\frac{\alpha\tanh\left(\frac{p_n}{\alpha}\right)}{p_n^5}\right]^{-1} \tag{10}$$

where μ is absolute viscosity, L is channel length, $2b$ is channel depth, α is channel aspect ratio (width over depth) and $p_n = (2n+1)\pi/2$ [25], and

$$I_s = \frac{\rho L}{4\alpha b^2} \tag{11}$$

where ρ is the mass density of the fluid [21].

In this study a more accurate expression for impedance was used. The impedance was derived from the exact solution to the Navier-Stokes equations for a harmonic oscillating pressure drop acting on incompressible fluid in a straight, rigid rectangular channel and is given by

$$\widehat{Z_v} = \frac{\mu L \pi^2}{32 b^4}\left[\sum_{n=0}^{\infty}\frac{1}{(2n+1)^2 q_n^2}\left(\alpha - \frac{\tanh(q_n\alpha)}{q_n}\right)\right]^{-1},$$
$$q_n = \sqrt{i\eta^2 + \frac{(2n+1)^2}{4}\pi^2} \tag{12}$$

where $\eta^2 = \rho b^2\omega/\mu$ is the nondimensional radian frequency. This expression is shown in [26] to be superior to the simplified case described by (9)–(11), particularly for $1 < \eta^2 < 1000$, i.e., around the cutoff frequency. It is perhaps not coincidental that all pumps involved in this study exhibited resonant behavior in this frequency range, thus underlining the importance of using the correct analytical methods.

TABLE I
GEOMETRIC DATA FOR STRAIGHT-CHANNEL DEVICES. THE PZT THICKNESS WAS 190 μm FOR ALL DEVICES. THE CHAMBER VOLUME INCLUDES HALF THE VOLUME OF EACH CHANNEL

device ID	chamber dia. mm	etch depth μm	chamber vol. mm^3	memb. thick. μm	PZT dia. mm
79	3	152	1.07	250	2.5
80	3	110	0.778	250	2.5
76	6	114	3.22	500	5.0
77	6	115	3.25	500	5.0
78	6	148	4.18	500	5.0

TABLE II
GEOMETRIC DATA FOR PUMPS WITH TESLA-TYPE VALVES CLASSIFIED BY GROUP. THE PZT THICKNESS WAS 190 μm FOR ALL PUMPS

group	pump ID	valve type	chamb. dia. mm	etch depth μm	memb. thick. mm	PZT dia. μm
1	81 82	IIb	3	109	165	2.5
2	83 84	IIa	6	138	165	5.0
3	89a 89b	IIa	6	105	500	5.0
4	87 88	I	6	141	500	5.0

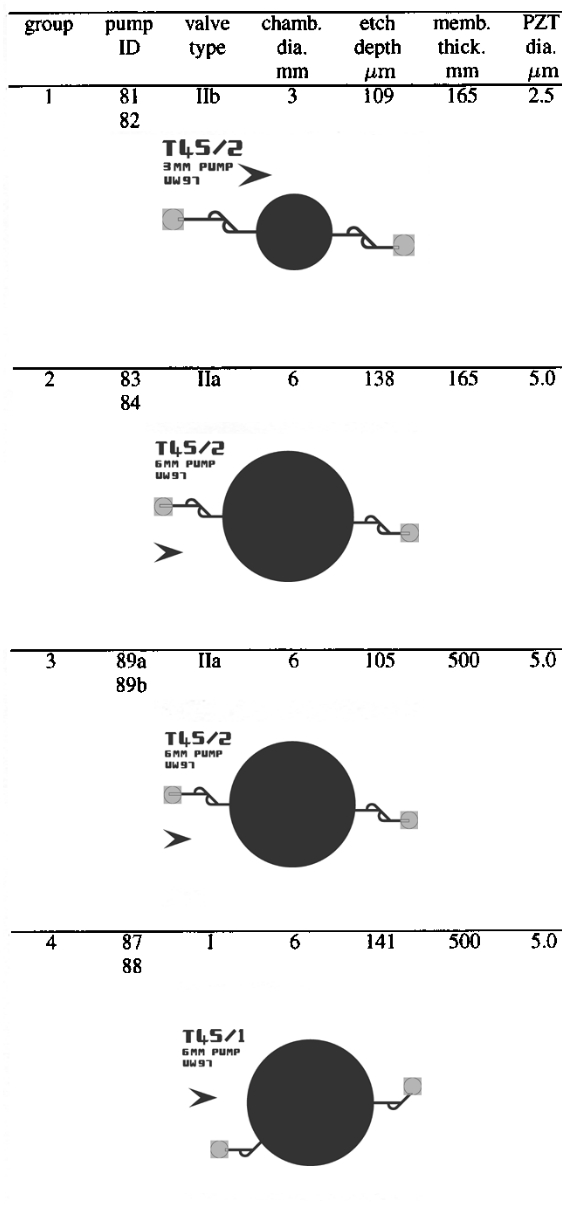

The above lumped-parameter representation for the valves is entirely determined by the length and transverse dimensions of a straight rectangular duct, density and absolute viscosity of the fluid and the frequency of oscillation. Since part of this study was directed toward determining the validity of this representation for actual valves in predicting pump resonant behavior, an approximation for the length L was necessary in order to use (12) for Tesla-type valves utilized on actual pumps considered. Two approximations were considered. In one case (L_{eq}) the length was based on a series-parallel network of valve segments as shown in Fig. 5. This approach was based on the assumptions that 1) the pressure drop across each branch in a parallel combination was the same, and 2) fully-developed oscillatory flow existed in all segments. In the other case (L_{ave}) it was based on the average of the shortest and longest path through the valve as shown in Fig. 5.

4) Fluidic Load Parameters: Fig. 3 shows four capacitors corresponding to the inlet and outlet regions of the pump system. Capacitors C_i and C_o correspond to on-chip capacitors [27], which were not incorporated into the pumps used in this study and were set to zero. Capacitors C_{ti} and C_{to} correspond to open reservoirs to which a pump was attached. A value of approximately 10^{-10} m^3/Pa was used for both reservoirs. This value corresponds to the capacitance $\pi D^2/4\rho g$ of a water reservoir 1 mm in diameter. This value was large enough that calculated membrane centerline velocity amplitude was essentially insensitive to the exact value and equivalent to constant pressure at the distal ends of R_{vi} and R_{vo}.

B. Experimental Devices

Micropumps like the one shown in Fig. 1 and "micropump-like" devices with straight-channels replacing valves like the one shown in Fig. 6 were utilized in this study. The valves (or channels) and pump chambers were etched together using deep reactive ion etching (DRIE). The etch depth of each device was measured in the pump chamber using an optical interference measurement system (Fotonic MTI-2000, MTI Instruments, Albany, New York).

The straight-channel devices were utilized to test the theoretical predictions of the resonant behavior under conditions most faithful to the model and to investigate the effects of fluid compliance. Most characteristics of these devices are summarized in Table I. For all these devices the channels were 120 μm wide and 1.37 mm long for the 3 mm chamber; 2.24 mm long for the 6 mm chamber. A Pyrex cover (the membrane) was anodically bonded to the top, and a piezoelectric actuator was attached onto the Pyrex using electrically-conductive epoxy that was applied by hand with a brush. A 2-mm-thick Pyrex backing plate was anodically bonded to the back of each device. Holes were drilled through the backing plate and silicon for inlet and outlet connections. By measuring the thickness of the individual components before and after attaching the piezoelectric actuator, it was determined that the nominal thickness of the epoxy layer was 20 μm.

Four types of micropumps with Tesla-type valves were utilized and are summarized in Table II. These pumps were identical in fabrication to the straight channel devices described above. All valves consisted of conduits 114 μm wide. Details of the valve geometry are given in Table III.

The groups indicated in Table II were used to study several aspects of design parameters. The pumps in groups 2 and 3 were

TABLE III
GEOMETRY FOR TESLA-TYPE VALVES. SEE TABLE II AND FIG. 5 FOR THE DEFINITION OF TERMS

Valve Type	L_{eq} mm	L_{avg} mm
I	1.43	1.90
IIa	1.91	2.64
IIb	2.13	3.03

TABLE IV
VALUES OF ELECTRO-MECHANICAL PARAMETERS CALCULATED WITH FINITE ELEMENT ANALYSIS. THE THREE CASES SHOWN COVER ALL COMBINATIONS OF CHAMBER DIAMETER AND MEMBRANE THICKNESS STUDIED. CASE A: 3 mm AND 165 μm, CASE B: 3 mm & 250 μm, CASE C: 6 mm AND 165 μm, CASE D: 6 mm AND 500 μm

case	$f_e \times 10^9$ m/V	$k \times 10^{-6}$ N/m	γ	$m \times 10^5$ kg	$(C_c)_h \times 10^{18}$ $\mathrm{m^3/Pa}$
A	3.06	4.61	0.414	0.460	0.108
B	2.31	7.89	0.414	0.508	0.0969
C	12.6	1.37	0.417	1.53	2.93
D	4.37	8.56	0.432	2.18	1.61

the same except for membrane thickness, affecting primarily the mechanical parameters k and f_e. The pumps in groups 3 and 4 differed only with respect to the valves. Valve type I refers to a single-cell Tesla-type element, and valve type II refers to double-cell Tesla-type elements. The pumps in groups 1 and 2 were essentially the same except for the chamber diameter, which affected C_c and the mechanical parameters k and f_e, and this, in conjunction with groups 2 and 3, was used to investigate chamber compliance.

C. Experimental Procedures

For resonance tests with only air in the pumps, each pump was flushed with ethanol, then water, and finally compressed air. For measurements with liquid, each pump was connected to inlet and outlet reservoirs by 15 cm long, 1 mm diameter Silastic tubing. Each pump was primed with ethanol, which was then displaced with deionized water that was filtered to 0.2 μm and degassed with a vacuum pump (model N810.3FT8, KNF Neuberger, Inc., Trenton, NJ) for 10 min at 29 inHg vacuum. The chamber was visually inspected for air bubbles, and the valves were visually inspected for debris on an inverted optical microscope (IM35, Zeiss, Germany). The ambient temperature for all tests was 25 ± 1 °C.

The resonant behavior of the pumps was investigated by measuring the membrane centerline velocity using a laser vibrometer (Model OVF 302, Polytec, Waldbronn Germany) while a signal generator (Model 19, Wavetek, U.K.) applied a harmonic input voltage to the pump actuator. Voltage levels were chosen high enough to acquire a good velocity signal, low enough to minimize entrance effects in the straight channels and were in the range of approximately 5–25 V [26].

III. RESULTS AND DISCUSSION

The electro-mechanical parameters calculated from finite element analysis and used to determine the discrete elements of the system model are summarized in Table IV. The cases shown apply to both the straight-channel devices and the pumps with Tesla-type valves.

TABLE V
MEASURED AND CALCULATED FREE-AIR RESONANCE OF STRAIGHT-CHANNEL DEVICES

device ID	measured frequency kHz	calculated frequency kHz	deviation from calculated %
79	196	198	-0.91
80	192	198	-2.8
76	104	99.7	+3.7
77	101	99.7	+1.3
78	103	99.7	+2.9

A. Devices With Straight-Channel Valves

The straight-channel devices were first tested dry to determine how well the dynamic behavior compared with the finite element analysis without the effects of chamber and valves. Table V is a comparison of measured resonant frequency with that calculated from finite element analysis. The discrepancies were less than five percent, which demonstrated that the mechanical values f_e, k, γ and m given in Table IV were accurately determined, all based on first principles. It also demonstrated that the effect of air on pump behavior was negligible.

The straight-channel devices were next tested filled with water. Based on the results from the dry tests, the comparison of measurement and model prediction for liquid-filled devices was used to determine the accuracy of the remaining elements, C_c, R_v and I_v. The reason for investigating straight-channel devices was to have the ability to model R_v and I_v as accurately as possible. Also, given that the results from the dry tests were in good agreement with model predictions, we assumed the remaining parameter $(C_c)_h$ in Table IV was accurately calculated. It was also considered reasonable that liquid compliance due to the bulk modulus β of liquid was accurately modeled since β for water does not vary significantly with temperature or pressure. Only the gas fraction ϕ was not known *a priori*. The tests performed were based on the fact that if ϕ were constant, the fluid chamber compliance would be linear with chamber volume according to (8). The devices were operated at a low voltage such that the Reynolds number in the straight channels was low enough to neglect entry/exit losses [26]. The frequency response of the membrane centerline velocity was compared to model predictions with ϕ adjusted so that the model and experimental resonant frequency matched. Figs. 7 and 8 show the results for the 3 mm and 6 mm devices, respectively. With the values of ϕ obtained from these experiments, (8) was used with P_c taken as atmospheric pressure to plot $(C_c)_f$ versus chamber volume as shown in Fig. 9. Indeed the relationship was linear and a least squares fit to the data yielded

$$(C_c)_f = \left(1.7151 \times 10^{-9} \frac{1}{\mathrm{Pa}}\right) V_c. \tag{13}$$

Based on the above relation and (8) for a chamber at atmospheric pressure, i.e., a pump operating against no pressure head, a

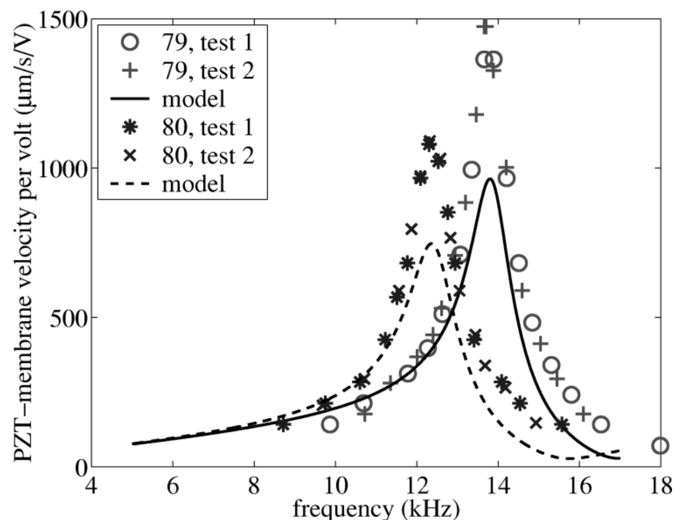

Fig. 7. Membrane centerline velocity frequency response for two 3-mm-diameter straight-channel devices with different etch depths given in Table I. Shown are results for each device taken on two different days. Actuation levels were approximately 4 V peak-to-peak. Model predictions correspond to a volumetric gas fraction of 0.022% and 0.025% for devices 79 and 80, respectively.

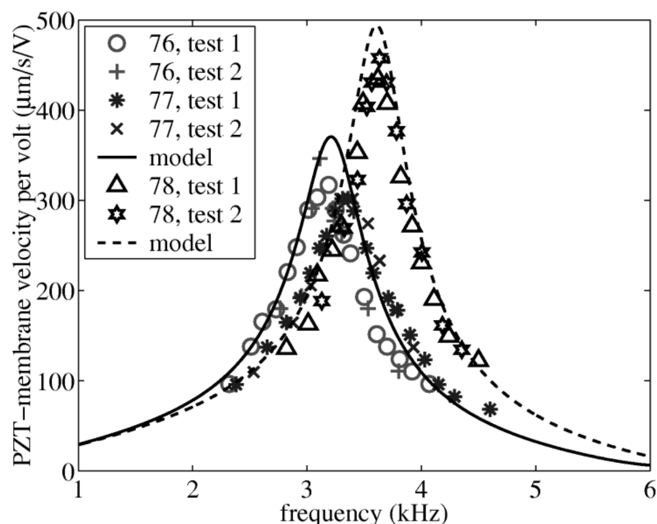

Fig. 8. Membrane centerline velocity frequency response for three water-filled 6-mm diameter chambers with different etch depths given in Table I. Shown are results for each device taken on two different days. Actuation levels were approximately 4 V peak-to-peak. Model predictions correspond to a volumetric gas fraction of 0.019% for devices 76 and 77 and 0.017% for device 78.

constant value for the gas volume fraction was calculated to be

$$\phi = 0.00018. \qquad (14)$$

Equation (14) is an important result of this study. Since the linear regression given by (13) was a good representation for the effect of gas in the pumped liquid, the assumption that ϕ was constant for a given degassing protocol was sufficient to use the value determined for this entire study. This was an important step since determining ϕ relied on the ability to accurately model the fluid behavior in the straight channels, something that is not as certain when applying (12) to Tesla-type valves, or any geometry other than straight rectangular channels.

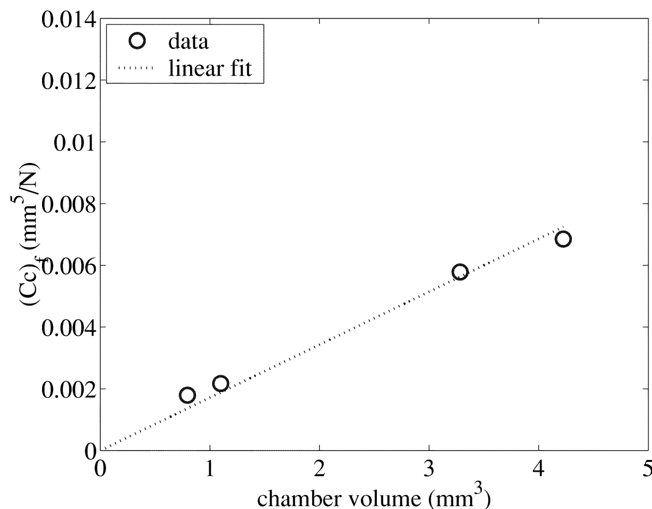

Fig. 9. Chamber capacitance due to fluid $(C_c)_f$ versus chamber volume for the four different chamber volumes investigated. Also shown is a linear regression that included the origin.

The agreement between model predictions and experiment shown in Figs. 7 and 8 justify the assumptions that R_c and I_c could be neglected and that it was reasonable to model the epoxy as an elastic material that did not contribute substantially to the overall dissipative behavior. It appears that the effect of viscous flow in the valves alone reasonably accounts for dissipation effects. This observation is also consistent with the equation for simplified flow resistance given by (10), which shows resistance is inversely proportional to the fourth power of the lateral dimensions of the valves. Thus, the dimensions of the valves resulted in their fluidic effect to be much more significant than that due to the chamber. This might not be the case for very shallow pump chambers.

To conclude this section on the straight-channel devices, it should be noted that the results presented were performed twice and on different days for all four devices. The variability between tests in all cases was small. In addition, the tests for virtually identically fabricated devices 76 and 77 also agreed well with each other. These results over repeated tests and on different devices of the same design further substantiated the results. It is also important to note that in the case of the 6 mm devices the agreement in amplitude response over the entire frequency range considered was excellent. Agreement was not as good with the 3 mm devices, and possibly indicated that small differences in fabrication of the smaller devices might have resulted in larger variations in resonant behavior. This is especially applicable in this case since these prototypes were hand-assembled.

B. Pumps With Tesla-Type Valves: Resonant Behavior

The primary goal for investigating pumps with Tesla-type valves was to investigate use of the linear model for pumps with actual valves, for which the method of determining R_v and I_v is only an approximation. In that case any additional differences between model and experiment from that observed for the straight-channel devices *could only be attributed to this approximation*. Reasonable agreement would show that, despite the approximation, the method described would be suitable for

TABLE VI
MEASURED AND CALCULATED FREE-AIR RESONANCE OF PUMPS WITH TESLA-TYPE VALVES. DEVICE 81 WAS CONSIDERED TO BE AN OUTLIER

device ID	measured frequency kHz	calculated frequency kHz	deviation from calculated %
81	121	159	-24
82	150	159	-5.8
83	45.5	47.5	-4.1
84	44.5	47.5	-6.4
89a	100	99.7	+0.60
89b	106	99.7	+6.0
87	100	99.7	+0.40
88	105	99.7	+5.1

TABLE VII
VALVE PARAMETERS FOR WATER-FILLED TESLA-TYPE VALVES. THE NOTATION f_{op} DENOTES THE OPERATING FREQUENCY AT WHICH THE PARAMETERS WERE DETERMINED. THE VALUES CORRESPOND TO L_{eq} DEFINED IN FIG. 5 AND TABULATED IN TABLE III

group	f_{op} kHz	$R_v \times 10^{-11}$ kg/m^{4}s	$I_v \times 10^{-8}$ kg/m^4
1	9.0	11.2	1.88
2	1.7	3.54	1.46
3	3.5	7.21	1.85
4	4.0	3.59	1.01

calculation of all parameters including valve *size* for optimum resonant behavior based on first principles alone.

As was done with the straight-channel devices, free-air resonant behavior of the pumps was first investigated to determine whether each pump was fabricated consistently. The comparison of measured membrane resonant frequency with that predicted by finite element analysis is shown in Table VI. The ANSYS predictions were within seven percent of the experimentally-measured resonant frequency for all pumps except the 3 mm pump 81, which exhibited a 24 percent difference. The difference between the two 3 mm pumps could not be explained. Given the overall agreement between measured and calculated values, pump 81 was considered to be an outlier compared to the other pump of the same design.

For the case of liquid-filled pumps, the valve parameters used in the system model were calculated based on (9) and are given in Table VII. Since resistance and inertance are functions of frequency based on the exact solution of the Navier-Stokes equations, the frequency used corresponded to the resonant frequency predicted by the model once all other parameters were input. This approach required an iterative application of the linear model.

Figs. 10 through 13 show experimental data and linear model predictions for membrane velocity amplitude as a function of frequency. In some cases multiple tests are presented for the same pump to indicate variations between tests. Except for the 3 mm pumps the agreement between the pump pairs that were fabricated from the same design were in reasonable agreement. This was particularly true for groups 2 and 3. The disagreement in experimental results for the two 3 mm pumps was expected based on the free-air resonance tests reported earlier, from which pump 81 was considered an outlier.

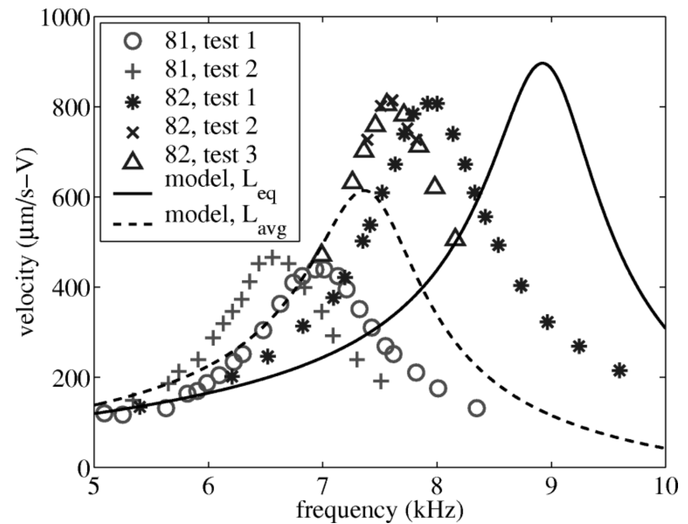

Fig. 10. Results for two 3 mm pumps compared with model predictions (group 1 from Table II. Actuation was 8–20 V peak-to-peak. Model predictions are given for both $L_{\rm eq}$ and $L_{\rm avg}$ defined in Fig. 5.

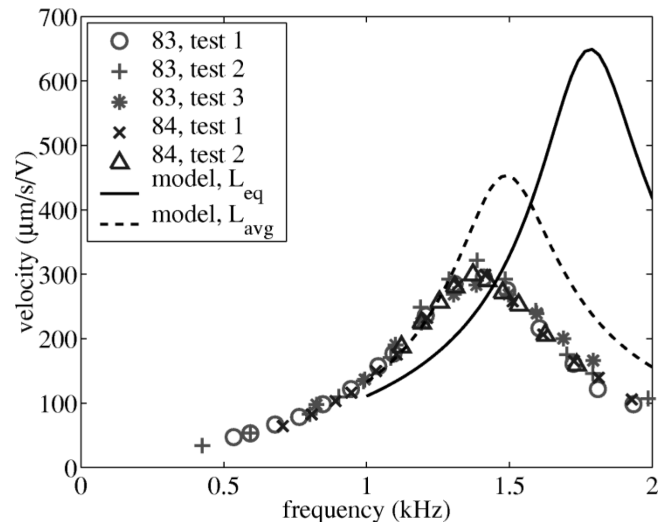

Fig. 11. Results for two 6 mm pumps compared with model predictions (group 2 from Table II). Actuation was 5–25 V peak-to-peak. Model predictions are given for both $L_{\rm eq}$ and $L_{\rm avg}$ defined in Fig. 5.

Common to all four groups was that model predictions based on $L_{\rm eq}$ were high in terms of both frequency and magnitude. This was different from the results for the free-air resonant behavior for which the resonant frequency predicted by the model was both above and below the measured values. This trend was most likely due to the approximation of the straight-channel analytical solution for the actual dynamic fluid behavior. Since both the resonant frequency and amplitude of the model decrease with increase in resistance and inertance, an alterative length $L_{\rm avg}$ was considered (see Fig. 5 and Table III) and shown in the figures as dashed lines. The results based on $L_{\rm avg}$ were in error as much as those based on $L_{\rm eq}$ but without an apparent trend in amplitude and frequency. Based on both length definitions, the agreement between measurement and model was on the order of 20%. Since both lengths were ad hoc definitions, the intention of these results is to indicate the variance rather than justification for using one length or the other.

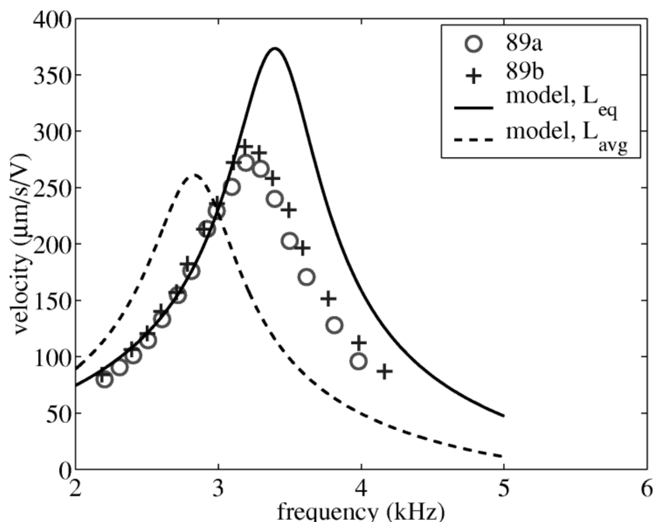

Fig. 12. Results for two 6 mm pumps compared with model predictions (group 3 from Table II). Actuation was 20–25 V peak-to-peak. Model predictions are given for both $L_{\rm eq}$ and $L_{\rm avg}$ defined in Fig. 5.

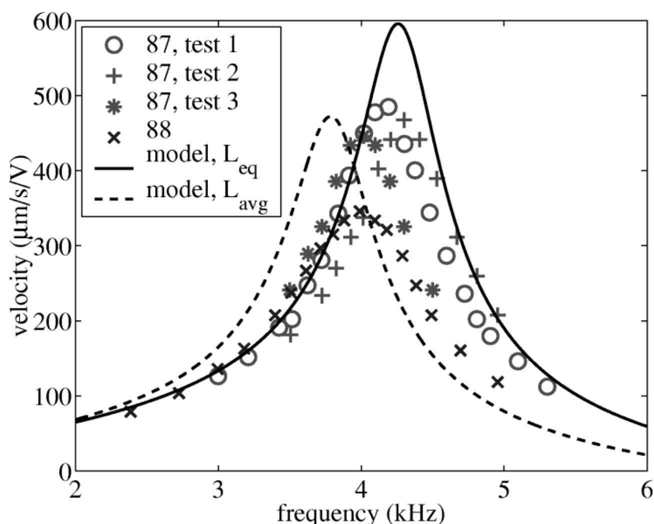

Fig. 13. Results for two 6 mm pumps compared with model predictions (group 4 from Table II). Actuation was 16–23 V peak-to-peak. Model predictions are given for both $L_{\rm eq}$ and $L_{\rm avg}$ defined in Fig. 5.

Given the reasonably accurate agreement between linearized model for straight channel devices and actual pumps as demonstrated above, consideration of the large numbers of parameters that influence resonance can be investigated as an efficient design methodology for micropumps with fixed valves. As an example, Figs. 14 and 15 show 975 different combinations of membrane thickness and valve size determined with the linear model. The design space of membrane thickness and valve width shown includes the parameters of device #80 (see Table I), except that for each membrane thickness piezoelectric element dimensions (diameter and thickness) were optimized with FEA for maximum deflection per volt, and the valve length to width ratio was held fixed and equal to 15. Performance predictions must take into account peak volume flow rate and peak Reynolds number. This is shown in Fig. 15, which clearly shows a result that is not readily apparent from the surface for membrane velocity in Fig. 14. These examples

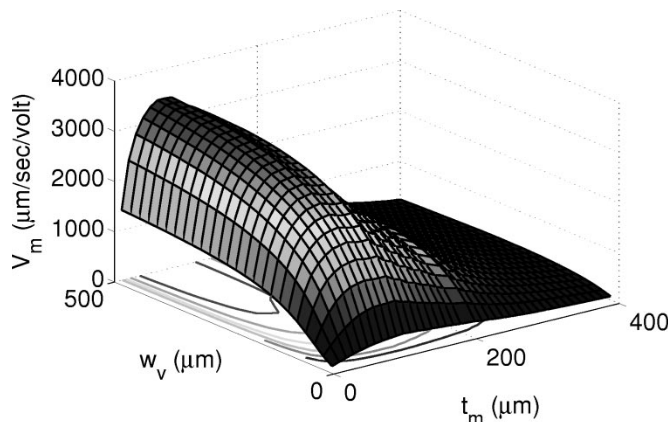

Fig. 14. Membrane peak centerline velocity versus membrane thickness t_m and valve width w_v.

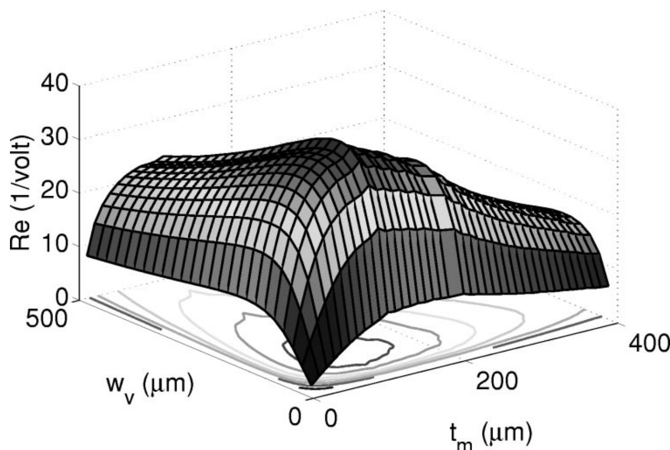

Fig. 15. Peak Reynolds number versus membrane thickness t_m and valve width w_v.

indicate the direction of future work utilizing the linear model to optimize the multitude of pump parameters, including valve *size*. In addition, methods for optimizing valve *shape*, such as [28], and experimental verification of the overall optimization approach are needed.

IV. Conclusion

A model for fixed-valve micropumps was presented in this study based on first principles, with no experimental or otherwise empirical information needed to predict resonant behavior. Agreement between model and experiment was excellent for fixed-valve micropumps when valves were replaced by straight channels. The agreement between the linear model and pumps with Tesla-type valves was reasonable with errors on the order of 20%. This error was entirely attributable to the straight-channel approximation of the valve fluidics. Yet the agreement is sufficient to use the model to design pumps for optimum resonant behavior by adjusting any desired geometric or material parameter.

The design methods presented make possible the determination of optimal valve *size*. In order to determine optimal valve *shape*, and predict optimal pump performance in terms of net pressure and flow, additional analysis of the valve fluid dynamics is required. The principles in this study are critical to

future analyzes, because it was clearly demonstrated that except for the nonlinear aspects of fixed-geometry valves, all parameters of the dynamic model can be accurately calculated from first principles.

REFERENCES

[1] M. C. Carrozza, N. Croce, B. Magnani, and P. Dario, "A piezoelectric-driven stereolithography-fabricated micropump," *J. Micromech. Microeng.*, vol. 5, no. 2, pp. 177–179, 1995.

[2] M. Koch, N. Harris, R. Maas, A. G. R. Evans, N. M. White, and A. Brunnschweiler, "A novel micropump design with thick-film piezoelectric actuation," *Meas. Sci. Technol.*, vol. 8, pp. 49–57, 1997.

[3] R. Linnemann, P. Woias, C.-D. Senfft, and J. A. Ditterich, "A self-priming and bubble-tolerant piezoelectric silicon micropump for liquids and gases," in *Proc. Micro Electro Mechanical Systems, MEMS '98*, Heidleberg, Germany, Jan. 25–29, 1998, pp. 532–537.

[4] T. Bourouina, A. Bossebœuf, and J.-P. Grandchamp, "Design and simulation of an electrostatic micropump for drug-delivery applications," *J. Micromech. Microeng.*, vol. 7, pp. 186–188, 1997.

[5] S. Böhm, M. Dierselhuis, W. Olthuis, and P. Bergveld, "Manufacturing of self-priming plastic micropumps," in *Proc. Micro Total Analysis Systems '98*, Banff, Canada, 1998, pp. 391–394.

[6] E. Stemme and G. Stemme, "A valveless diffuser/nozzle-based fluid pump," *Sens. Actuators, Phys. A*, vol. 39, pp. 159–167, 1993.

[7] T. Gerlach and H. Wurmus, "Working principle and performance of the dynamic micropump," *Sens. Actuators, Phys. A*, vol. 50, pp. 135–140, 1995.

[8] F. Forster, R. Bardell, M. Afromowitz, and N. Sharma *et al.*, "Design, fabrication and testing of fixed-valve micropumps," in *Proc. ASME Fluids Engineering Division, 1995 ASME International Mechanical Engineering Congress and Exposition*, vol. 234, D. C. Wiggert *et al.*, Eds., San Francisco, CA, Nov. 12–17, 1995, pp. 39–44.

[9] F. K. Forster, R. L. Bardell, A. P. Blanchard, M. A. Afromowitz, and N. R. Sharma, "Micropumps With Fixed Valves," U.S. Pat. 5 876 187, Mar. 2, 1999.

[10] N. Tesla, "Valvular Conduit," U.S. Patent 1 329 559, 1920.

[11] L.-S. Jang, C. J. Morris, N. R. Sharma, R. L. Bardell, and F. K. Forster *et al.*, "Transport of particle-laden fluids through fixed-valve micropumps," in *Proc. Micro-Electro-Mechanical Systems (MEMS), 1999 ASME International Mechanical Engineering Congress and Exposition*, vol. MEMS-1, A. P. Lee *et al.*, Eds., Nashville, TN, Nov. 14–19, 1999, pp. 503–509.

[12] L.-S. Jang, N. R. Sharma, and F. K. Forster, "The effect of particles on the performance of fixed-valve micropumps," in *Micro Total Analysis Systems 2000*, A. van den Berg, W. Olthuis, and P. Bergveld, Eds., Enschede, May 14–18, 2000, pp. 283–286.

[13] P. Voigt *et al.*, "Electrofluidic full-system modeling of a flap valve micropump based on kirchoffian network theory," *Sens. Actuators, Phys. A*, vol. 66, pp. 9–14, 1998.

[14] T. Bourouina and J. Grandchamp, "Modeling micropumps with electrical equivalent networks," *J. Micromech. Microeng.*, vol. 6, no. 4, pp. 398–404, 1996.

[15] M. Carmona *et al.*, "Dynamic simulations of micropumps," *J. Micromech. Microeng.*, vol. 6, pp. 128–130, 1996.

[16] A. Olsson, P. Enoksson, G. Stemme, and E. Stemme, "A valve-less planar pump in silicon," in *Proc. Transducers '95 Eurosensors IX*, vol. 2, Stockholm, Sweden, 1995, ISBN 91-630-3473-5, pp. 291–294.

[17] A. Ullman, "The piezoelectric valve-less pump-performance enhancement analysis," *Sens. Actuators, Phys. A*, vol. 69, pp. 97–105, 1998.

[18] A. Olsson *et al.*, "A numerical design study of the valveless diffuser pump using a lumped-mass model," *J. Micromech. Microeng.*, vol. 9, no. 1, 1999.

[19] R. Bardell, R. Sharma, F. K. Forster, M. A. Afromowitz, and R. Penney *et al.*, "Designing high-performance micro-pumps based on no-moving-parts valves," in *Proc. Micro-Electro-Mechanical Systems (MEMS), 1997 ASME International Mechanical Engineering Congress and Exposition*, vol. DSC-234/HTD-354, L. Lin and K. E. Goodson, Eds., Dallas, TX, Nov. 16–21, 1997, pp. 47–53.

[20] F. K. Forster, R. L. Bardell, and N. R. Sharma, "Method for Making Micropumps," U S. Pat. 6 227 809, May 8, 2001.

[21] D. Rowell and D. N. Wormley, *System Dynamics: An Introduction*. Upper Saddle River, NJ: Prentice Hall, 1997.

[22] C. J. Morris and F. K. Forster, "Optimization of a circular piezoelectric bimorph for a micropump driver," *J. Micromech. Microeng.*, vol. 10, no. 3, pp. 459–465, 2000.

[23] C. Y. K. Chee, L. Tong, and G. P. Steven, "A review on the modeling of piezoelectric sensors and actuators incorporated in intelligent structures," *J. Intell. Mater. Syst. Struct.*, vol. 9, pp. 3–19, Jan. 1998.

[24] W. A. Brantley, "Calculated elastic constants for stress problems associated with semiconductor devices," *J. Appl. Phys.*, vol. 44, no. 1, pp. 534–535, 1973.

[25] F. M. White, *Viscous Fluid Flow*, 3rd ed. New York: McGraw-Hill, 1991.

[26] C. J. Morris and F. K. Forster, "The correct treatment of harmonic pressure-flow behavior in microchannels," in *Proc. Micro-Electro-Mechanical Systems (MEMS), 2000 ASME International Mechanical Engineering Congress and Exposition*, vol. MEMS-2, Orlando, FL, Nov. 5–10, 2000, pp. 473–479.

[27] T. T. Veenstra, N. R. Sharma, F. K. Forster, J. G. E. Gardeniers, M. C. Elwenspoek, and A. van den Berg, "The design of an in-plane compliance structure for microfluidical systems," *Sens. Actuators, Chem. B*, vol. 81, no. 2–3, pp. 377–383, 2002.

[28] F. K. Forster and B. E. Williams, "Parametric design of fixed-geometry microvalves—the Tesser valve," in *Proc. 2002 ASME International Mechanical Engineering Congress and Exposition (IMECE 2000), Fluids Engineering, Microfluidics*, vol. 1, New Orleans, LA, Nov. 17–22, 2002, Paper IMECE 2002-33 628, (CD-ROM).

Christopher J. Morris received the B.S. and M.S. degrees in mechanical engineering from the University of Washington, Seattle, in 1998 and 2000, respectively.

From 1998 to 2001, he worked as Research Assistant at the University of Washington, focusing on the development of micropumps. He has worked at Micronics, Inc. for nearly two years with laser-cut, laminated plastic, microfluidic devices. He has modeled, built, and tested many versions of these devices for numerous medical diagnostic and life sciences applications.

Mr. Morris is a Member of the American Society of Mechanical Engineers (ASME).

Fred K. Forster received the B.S. degree in aeronautical and astronautical engineering from the University of Illinois, Urbana, and the M.S. and Ph.D. degrees in aeronautics and astronautics from Stanford University, Stanford, CA.

While at Stanford University, he held a position at the Lockheed Missiles and Space Company. Before coming to the University of Washington, Seattle, as a Postdoctoral Fellow, he was a Research Fellow at the Institut für Biomedizinische Technik an der Universität und ETH, Zürich, Switzerland. His is currently Associate Professor of Mechanical Engineering at the University of Washington. His research interests include fluid mechanics and acoustics applied to medicine and microfluidics.

Prof. Forster has served as Technical Committee Chair for the Microfluidics Symposium of the ASME IMECE for 1998–2000 and currently is the first Chair of the ASME Fluids Engineering Division Micro and Nano Fluid Dynamics Technical Committee. He is also an Associate Editor for the IEEE/ASME JOURNAL OF MICROELECTROMECHANICAL SYSTEMS. He is a Member of the American Society of Mechanical Engineers (ASME).